Journal of Molecular and Cellular Cardiology 123 (2018) 75–87

Contents lists available at ScienceDirect

Journal of Molecular and Cellular Cardiology

journal homepage: www.elsevier.com/locate/yjmcc

Original article

Reduction of cardiac TGFβ-mediated profibrotic events by inhibition of Hsp90 with engineered protein

Cáceres R.A.[a,f], Chavez T.[a,f], Maestro D.[a], Palanca A.R.[a,b], Bolado P.[a], Madrazo F.[c], Aires A.[d], Cortajarena A.L.[d,e], Villar A.V.[a,*]

[a] Instituto de Biomedicina y Biotecnología de Cantabria (IBBTEC), CSIC-Universidad de Cantabria, Santander, Spain
[b] Departamento de Anatomía y Biología Celular, Universidad de Cantabria, Santander, Spain
[c] Instituto de Investigación Marqués de Valdecilla (IDIVAL), Santander, Spain
[d] CIC biomaGUNE, Parque Tecnológico de San Sebastián, 20014 Donostia-San Sebastián, Spain
[e] Ikerbasque, Basque Foundation for Science, Mª Díaz de Haro 3, 48013 Bilbao, Spain
[f] Universidad Nacional de San Agustín de Arequipa, Perú

ARTICLE INFO

Keywords:
Consensus tertratricopeptide repeat (CTPR)
Designed proteins
Hsp90/ Hsp90 protein inhibitor
Myocardial fibrosis
TGFβ signaling

ABSTRACT

Myocardial fibroblast activation coupled with extracellular matrix production is a pathological signature of myocardial fibrosis and is governed mainly by transforming growth factor TGFβ-Smad2/3 signaling. Targeting the ubiquitous TGFβ leads to cellular homeostasis deregulation with adverse consequences. We previously showed the anti-fibrotic effects upon downregulation of 90-kDa heat shock protein (Hsp90), a chaperone that associates to the TGFβ signaling cascade. In the present study, we use a fluorescent-labeled Hsp90 protein inhibitor (CTPR390–488) with specific Hsp90 binding properties to reduce myocardial pro-fibrotic events in vitro and in vivo. The mechanism of action involves the disruption of TGFβRI-Hsp90 complex, resulting in a decrease in TGFβ signaling and reduction in extracellular matrix collagen. In vivo, decreased myocardial collagen deposition was observed upon CTPR390–488 treatment in a pro-fibrotic mouse model. This is the first study demonstrating the ability of an engineered Hsp90 protein inhibitor to block collagen expression, reduce the motility of myocardial TGFβ-activated fibroblasts and ameliorate angiotensin-II induced cardiac myocardial fibrosis in vivo.

1. Introduction

Myocardial fibrosis is a common phenomenon in the late stages of diverse cardiac diseases and it is a predictive factor of poor cardiac recovery. The mechanical cues are known to activate cardiac fibroblasts resulting in their differentiation into myofibroblasts, proliferation and excessive extracellular matrix production and long-term matrix stiffening. These events result in structural and functional alterations of the heart. Myocardial fibrosis lacks an effective treatment; approaches to reduce fibrosis exploit the understanding of the fibroblasts' role in the fibrotic process. Fibroblasts are the main contributors in the production of myocardial collagen principally through the transforming growth factor β (TGFβ) signaling pathway. TGFβ is the main pro-fibrotic cytokine. TGFβ exerts its effect by binding to a complex of TGFβ receptor I and II resulting in phosphorylation and translocation of Smad2/3 to the nucleus and increasing collagen production. Collagen protein deposition increases the extracellular matrix network [1–3]. The highly conserved ATP-dependent chaperone heat shock protein 90 (Hsp90) has been described as a component of the TGFβ signaling cascade [4–7]. The Hsp90 family consists mainly of four members: Hsp90aa1 or Hsp90α, Hsp90ab1 or Hsp90β, gp96 and TNF receptor associated protein 1 (TRAP1). The most important isoforms are the inducible Hsp90α, expressed upon stress stimuli, and the constitutively expressed isoform Hsp90β. Apart from its classical role in protein folding, Hsp90 binds other proteins, like transcription factors. In regards to the TGFβ signaling cascade, Hsp90 inhibition was described to attenuate renal fibrosis through degradation of TGFβ type II receptor [4]. Hsp90 inhibition was found to reduce collagen I synthesis on hepatic stellate cells (HSCs) in liver fibrosis [8]. Interesting data described by different groups including ours, showed that pharmacological and biological inhibition of Hsp90 effectively blocks the pro-fibrotic effects of TGFβ in different preclinical models of skin fibrosis in systemic sclerosis [6], in cardiac hypertrophy [9] or in cardiac fibrosis [10]. Hsp90 was presented as a novel modulator of TGFβ signaling in lung adenocarcinoma

* Corresponding author:
E-mail address: villarav@unican.es (A.V. Villar).

https://doi.org/10.1016/j.yjmcc.2018.08.016
Received 5 April 2018; Received in revised form 6 August 2018; Accepted 17 August 2018
Available online 05 September 2018

and bronchoalveolar carcinoma cells [5]. Various Hsp90 inhibitors such as geldanamycin, radicicol, 17-AAG, 17-DMAG, AUY-922, AT-13387, STA-9090, CNF-2024 are used to block Hsp90 activity in cancer with numerous side effects due to the inhibition of the ATPase domain, a key functional element in its Hsp90's protein folding activity [11].

A new class of small protein therapeutic agents have been described, derived from natural binding domains including ankyrin repeats, tetratricopeptide repeats, and other protein scaffolds [12–14]. Of particular interest is a previously designed Hsp90 binding module based on a tetratricopeptide repeat scaffold (CTPR390) that aims to inhibit Hsp90 minimizing the effects on cellular homeostasis [15] [16]. The engineered TPR scaffold is a protein generated by tandem repeats of a small structural motif (34 amino acids) with a simple architecture, stabilized by local interactions between the repeated modules [16]; its secondary and tertiary structures are characterized by the predominance of repeated and predictable local interactions. Therefore, there is a clear structural and functional delimitation between key residues encoding the stability and the functionality of the protein module [17]. These consensus TPRs (CTPRs) are scaffold proteins that can act as small antibody mimetics into which different ligand recognition properties can be encoded [18], thus opening the door to multiple biotechnological and biomedical applications. CTPR390 specifically binds the MEEVD sequence at the C-terminal region of the Hsp90 protein, which represents the recognition sequence for Hsp90 co-chaperones [19]. A fluorophore (Alexa 488) was incorporated to the final biomolecule (CTPR390–488) for both in vitro and in vivo tracking.

One of the most studied in vivo small animal models developing myocardial fibrosis is the angiotensin II treated-mouse. The renin/angiotensin/aldosterone system plays an important role in normal myocardial function. However, chronic elevation in angiotensin II (Ang II) levels is associated with fibrosis among other pathological remodeling adverse effects [20]. TGFβ activation occurs downstream Ang II activity and implicates TGFβ–dependent collagen synthesis [21]. Ang II deregulation results in pathological remodeling, especially myocardial fibrosis [22], and its administration in animal models commonly induces left ventricular remodeling, progressive deterioration of cardiac function, and finally clinical syndrome of heart failure [23]. This mouse model of myocardial fibrosis was used to determine the effects of selective Hsp90 inhibition by the engineered protein CTPR390–488 on myocardial collagen synthesis and accumulation. We have previously pointed out the role for Hsp90 in sustaining TGFβ signaling and collagen synthesis in cardiac fibroblasts and also Datta et al. suggested that Hsp90 participates in cardiac remodeling in an in vivo model of cardiac fibrosis [7,9,10]. The novelty of this paper resides in the use of an engineered protein that does not act by inhibiting the ATPase activity of Hsp90 but by mimicking co-chaperone binding to Hsp90. This binding results in the inhibition of collagen synthesis preserving cellular homeostasis.

2. Results

2.1. CTPR390-488 is internalized in primary myocardial fibroblasts and does not affect cellular viability

In vivo confocal imaging experiments revealed the presence of CTPR390–488 inside and outside primary cardiac fibroblasts treated with two different concentrations (0.2 and 0.8 μM) of CTPR390-488 (Fig. 1A). Cell viability at increasing concentrations of CTPR390-488 was not affected (Fig. 1B). To assess the uptake efficiency of CTPR390-488 into primary cells, colorimetric and fluorometric assays were performed at 24 hours after CTPR390-488 addition. The average percentage of CTPR390–488 internalization at all concentrations tested (0.0, 0.1, 0.2, 0.4, 0.8, 1.5, and 3 μM) was 9.1 ± 3.3% measured by absorbance (Fig. 1C) or 9.3 ± 4.6%, when detected by fluorescence (Fig. 1D). The percentage of cellular uptake of the CTPR390-488 protein at each concentration was determined (Table 1 source data). Fig. 1E–1G show similar localization and distribution of the CTPR390–488 protein when detected by fluorometry and through immune-detection with the CTPR390-specific antibody in TGFβ-activated fibroblasts treated with 0.4 μM of CTPR390–488. Fig. 1H–1J show the WB detection and quantification of intra and extracellular CTPR390–488 protein in treated fibroblasts. The densitometric analysis of CTPR390–488 indicated that 7.72% was inside the cell after 24 h (Fig. 1J). These results showed that CTPR390–488 is efficiently internalized in primary cardiac fibroblasts without affecting the viability of the cells.

2.2. CTPR390-488-Hsp90 interaction does not reduce Hsp90 chaperone activity

We utilized fluorescence anisotropy to monitor the interaction between CTPR390–488 protein and the Hsp90 C-terminal peptide and determine the corresponding binding affinity (Fig. 2A). The results demonstrate that the capability of the protein to recognize the Hsp90 C-terminal peptide was not affected by the cysteine modification. Furthermore, the K_D value obtained for the interaction was 110 ± 7 μM, comparable to the value obtained previously [15]. Refolding assays were used to determine Hsp90 ATPase activity in the presence of increasing concentrations of CTPR390–488 in myocardial fibroblasts (Fig. 2B). We did not observe reduction on Hsp90 chaperone activity in any of the groups (WT control, Hsp90aa1 KO, WT + CTPR390–488, KO + CTPR390–488) at increasing concentrations of the inhibitor (0.1, 0.2, 0.4, 0.8 1.5 and 3 μM). We found significant increases in refolding activity when adding 0.4; 0.8 or 3 μM of CTPR390–488 compared to control fibroblasts ($*p < .05$). Rabbit reticulocyte lysate was used as positive control ($**p < .005$) and denatured luciferase in the absence of Hsp90 as negative control ($***p < .001$) (Fig. 2B). Gene expression of Hsp90aa1 slightly increased in WT fibroblasts with the CTPR390–488 treatment and Hsp90aa1 was not detected in Hsp90aa1 KO fibroblasts as expected (Fig. 2C). Gene expression of Hsp90ab1 was reduced in KO cells compared to WT fibroblasts (***p < .001) (Fig. 2D). The significant variations of Hsp90 chaperone activity were not due to changes in Hsp90 protein levels (Fig. 2E-2F). We did not find any Hsp90 overexpression in Hsp90aa1 KO cells treated with CTPR390–488 either (Fig. 2E-2F). Thus, the presence of CTPR390–488 did not alter the Hsp90 mRNA or protein expression, and the cellular effects observed in the presence of CTPR390–488 were not due to changes in Hsp90 expression. Activation of fibroblasts is ligand-dependent and TGFβ triggered Hsp90 mRNA and protein expression (Fig. S1) and collagen synthesis [10] in myocardial fibroblasts.

2.3. Co-localization of Hsp90 and CTPR390–488

CTPR390-488 is an engineered TPR-based protein domain with Hsp90 binding properties [15,24,25]. We previously reported, that the extracellular domain of TGFβRI seems to interact with the Hsp90 dimer, and both Hsp90 isoforms (α and β) can be secreted extracellularly and be part of the Hsp90 dimer [10]. Here, we observed the co-localization of Hsp90 and TGFβRI in primary fibroblasts extracted from the myocardium of WT mice cultured in the presence of TGFβ (0.3 ng/ml) (Fig. 3A-3D), and the co-localization of Hsp90 and CTPR390–488 (Fig. 3E-3I). We did not detect the triple co-localization (Hsp90/ TGFβRI/ CTPR390-488). We included in the Discussion a possible mechanism of action that disrupts Hsp90-TGFβRI complex due to the presence of CTPR390–488.

2.4. Collagen and p-Smad2/3 expressions were reduced in CTPR390-488-treated fibroblasts and fibroblasts from Hsp90aa1 KO mice

To explore the collagen production and TGFβ signaling activity in the presence of CTPR390–488, primary cardiac fibroblasts from WT mice were treated with CTPR390–488 (0, 0.1, 0.2 and 0.8 μM) and

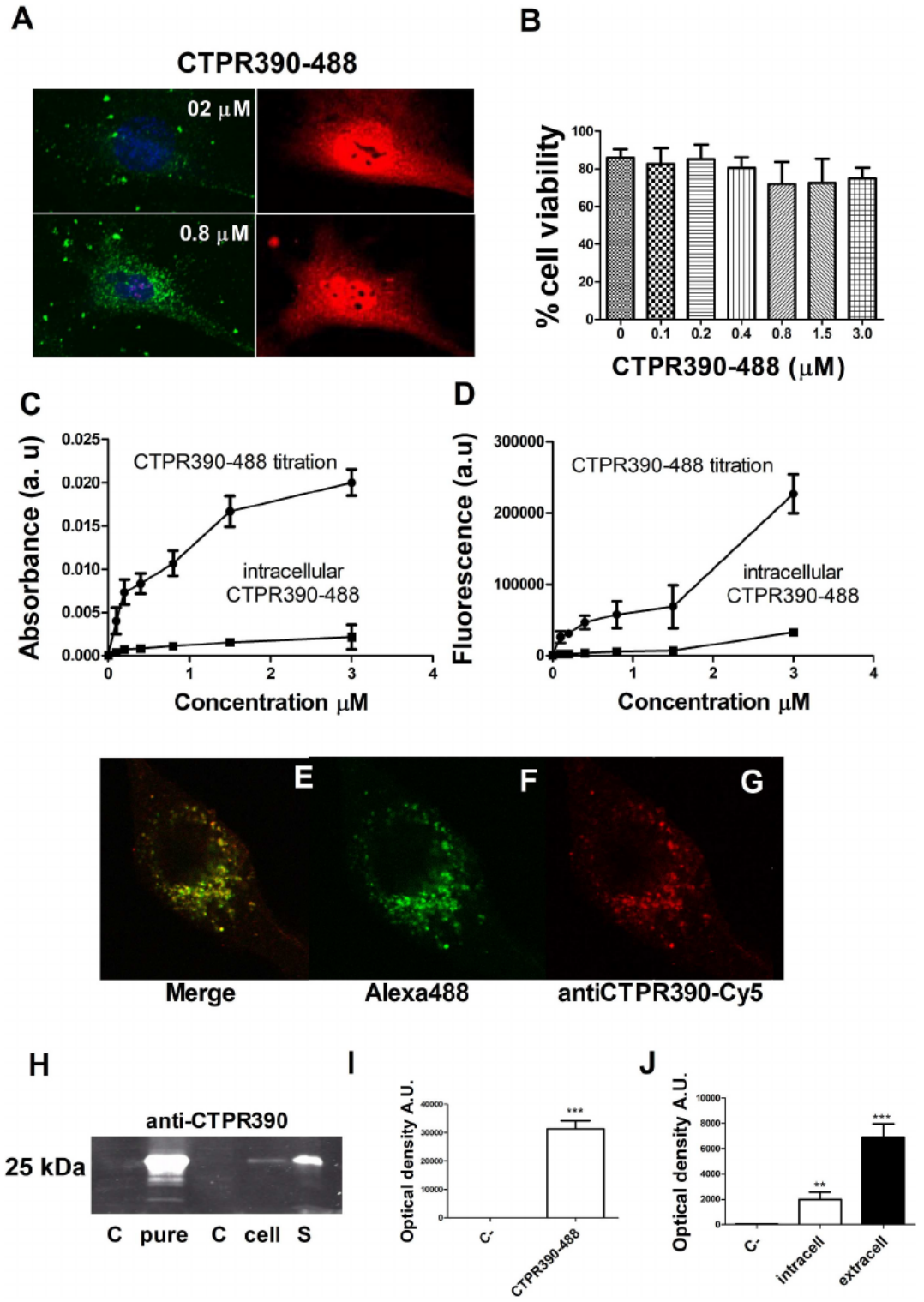

Fig. 1. CTPR390–488 detection in primary fibroblasts from WT mice myocardial tissue. A: Confocal microscopy showing the intrinsic fluorescence (green) of CTPR390–488 both intra and extracellularly at two different concentrations (0.2 and 0.8 μM) in living cells (not fixed). Right panels show the shape of the fibroblast in red. B: Cell viability at increasing concentrations of CTPR390–488. C, D: Absorbance and fluorescence values of a titration curve (pure CTPR390–488) and the correspondent CTPR390–488 signal at each concentration of intracellular samples. In all cases three independent experiments were performed. E, F, G: Co-localization of the two possible detection for CTPR390–488: its intrinsic Alexa 488 fluorescence and the CTPR390 immuno-detection. E: merge images of F and G. F: Confocal microscopy of the CTPR390–488 intrinsic fluorescence. G: the immunofluorescence detection of CTPR390–488 using anti-CTPR390 antibody and Cy5 secondary antibody. H: WB of the CTPR390–488 pure molecule (C), and CTPR390–488 from the fibroblasts lysate and the supernatant (S). I, J: quantification of CTPR390–488 WBs from (H). Significant variations of three independent experiments assayed were expressed vs. control (C), $*p < .05$, $**p < .005$, $***p < .001$; Mann–Whitney test. (For interpretation of the references to colour in this figure legend, the reader is referred to the web version of this article.)

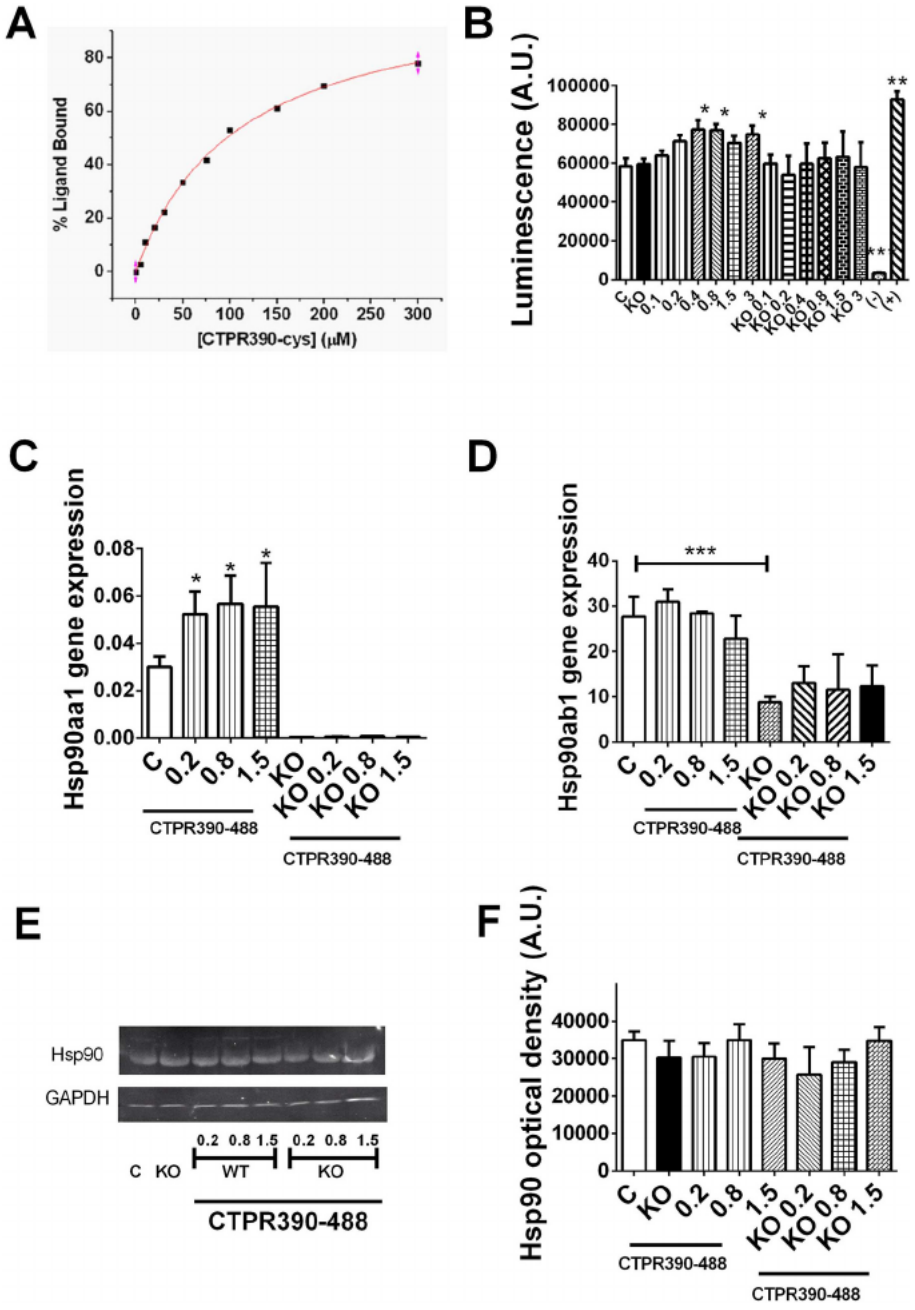

Fig. 2. Hsp90 binding and effect on Hsp90 chaperone activity of CTPR390–488. A: Fluorescein anisotropy assay showing Hsp90 binding activity of CTPR390–488 (K_D = 110 ± 7 μM). B: Hsp90-dependent refolding activity of lysates from WT and KO, myocardial fibroblasts adding CTPR390–488 different concentrations; the negative control (−) was denatured luciferase and the positive control (+) corresponded to rabbit reticulocyte lysate (RRL). C, D: Hsp90aa1 and Hsp90ab1 gene expressions in WT and Hsp90aa1 KO fibroblasts under increasing concentrations of CTPR390–488. E: Representative Western blot (WB) of Hsp90 expression in primary myocardial fibroblast of WT mice (C), Hsp90aa1 KO mice (KO) and WT and KO fibroblasts in the presence of different concentrations of CTPR390–488 (0.2; 0.8; 1.5 μM), GAPDH was used as control. F: Densitogram quantifying three independent experiments; data were expressed as mean ± SD of optical density in arbitrary units (A.U.). Significant variations of three independent experiments assayed were expressed vs. control (C), *p < .05, **p < .005, ***p < .001; Mann–Whitney.

compared to primary cardiac fibroblasts from Hsp90aa1 KO mice (Fig. 4). The results showed significant reduction in gene and protein expression for collagen I and collagen III upon treatment with increasing concentrations of CTPR390–488 (Fig. 4A-4D). The quantification of collagens from Hsp90aa1 KO cells also exhibited lower gene and protein expressions compared to WT control (Fig. 4A-4D). Collagen levels of Hsp90aa1 KO fibroblasts were also reduced upon treatment with CTPR390–488 compared to control KO cells (Fig. S2A-S2C). COL I deposition is lower in CTPR390–488-treated WT fibroblasts compared to control cells (Fig. 4E-4H). Immunofluorescence studies showed a higher area of collagen deposition in WT cells (Fig. 4F) than in CTPR390–488-treated cells (Fig. 4H). Quantification of the immunofluorescence results concluded that the collagen area (COL I) in WT cells (67.4% ± 6.5) was higher than in CTPR390–488 treated cells (36.9% ± 13.7 (**p < .005)) (Fig. 4I). The reduction of in vivo COL I deposition from Hsp90aa1 KO myocardial fibroblasts was previously described by our group [10]. Furthermore, TGFβ-induced Smad2/3 phosphorylation was reduced by the addition of CTPR390–488 (Fig. 4J-4K). TGFβRI was found to be a Hsp90 interacting protein [27] and Hsp90 inhibition can affect TGFβRI protein levels. Thus, we also analyzed the expression of TGFβRI and other Hsp90 well known interactors not directly related to the canonical Smad TGFβ signaling cascade (Akt, Erk and Hsp70) by Western blot analysis. Cardiac fibroblasts were treated with different doses of CTPR390–488, including doses effective in reducing collagen production. We did not observe differences in protein expression (Fig. S2D-S2J) of any of the tested Hsp90 interactors.

This result would sustain the ability of CTPR390–488 to maintain Hsp90 chaperone activity thus avoiding cellular homeostasis disruption. It has been shown that higher concentrations of CTPR390 (40 μM) induces a substantial decrease in the phosphorylation of Hsp90 client protein Her2 (p-Her2) in cancer cells [16]. Similar to those observations, the levels of the p-Smad2/3 was also diminished (Fig. 4K) as it were the phosphorylation levels of Akt and Erk (Fig. S2D, S2E, S2G). Akt and Erk activation are TGFβRI dependent in fibrotic processes, so

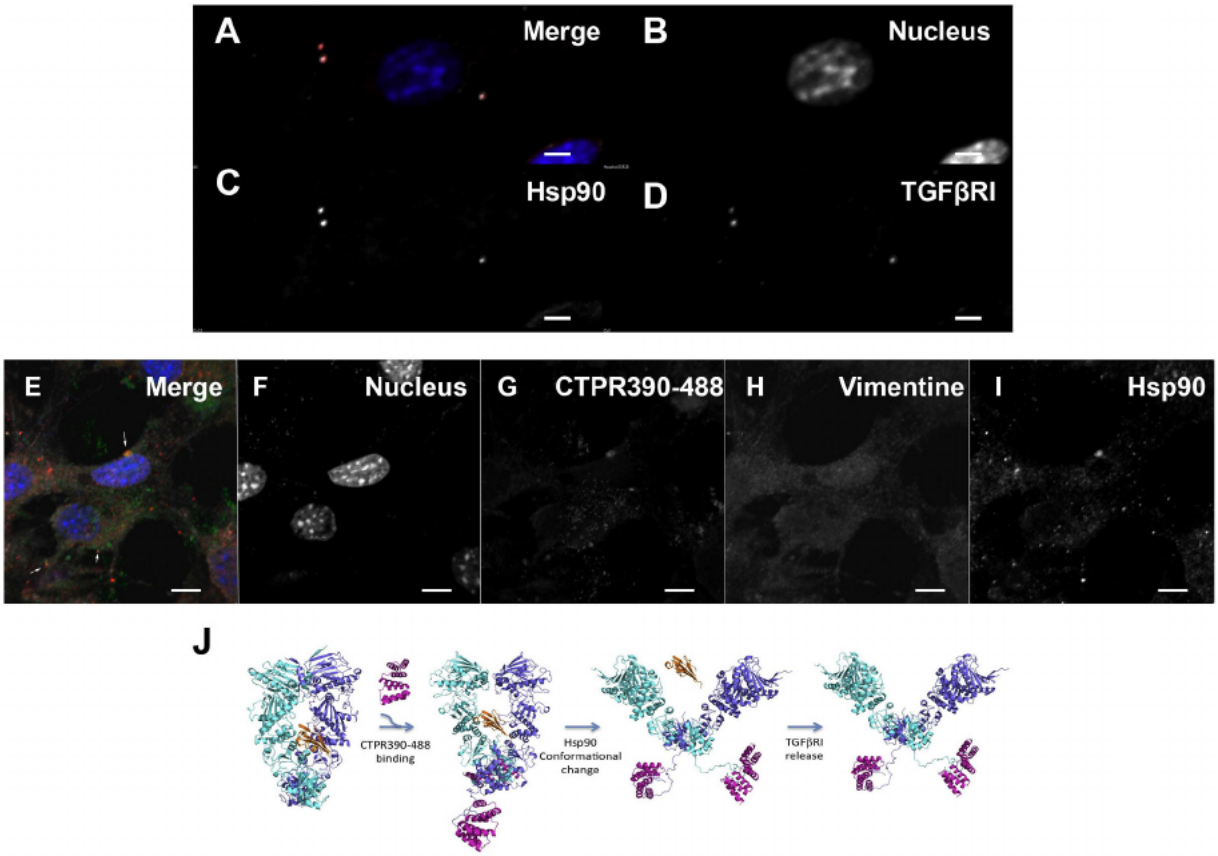

Fig. 3. Confocal microscopy assays showing protein co-localization in myocardial fibroblasts and in silico prediction of CTPR390–488 mechanism of action. A: merge-image showing co-localization of Hsp90 and TGFβRI. B: Hoechst was used as nuclear staining. C, D: Hsp90 is visualized with Cy3 and TGFβRI with Cy5 secondary antibodies. E: Co-localization of CTPR390–488 (green) and Hsp90 (red) in myocardial fibroblasts was detected in yellow and it was marked by white arrows. F: Hoechst was used as nuclear staining. G: intrinsic fluorescence of CTPR390–488 (green). H: vimentin marks the cellular shape (vimetin-Cy3 was placed in channel grey to merge the final image 3E with Image J software). I: Hsp90 is visualized with Cy5 secondary antibody and included in channel red of the Image J software to merge the final image 3E. Bar indicates 10 μm. J: From left to right: Molecular model of the interaction between the TGFβRI extracellular domain and Hsp90 closed dimer; Interaction of CTPR390–488 protein with the C-terminal end of Hsp90 domain; Hsp90 conformational change from the close to the open state upon CTPR390–488 interaction; disruption of the interaction between Hsp90 dimer (cyan and dark blue) and TGFβRI (orange). (For interpretation of the references to colour in this figure legend, the reader is referred to the web version of this article.)

its activation could be diminished by a reduction in TGFβRI effectiveness upon Hsp90 inhibition as it was shown for pulmonary fibrosis [28]. To show that CTPR390–488 indeed promoted inactivation of the TGFβ receptor complex, we transfected a constitutive active TGFβRI (TGFβRI-CA, kindly sent by Dr. Bartholin, TGFβ and Pancreatic Cancer – Lab Centre de Recherche en Cancérologie de LYON (CRCL)) and observed that CTPR390–488 was not able to influence pSmad2/3 or pErk expression (Fig. S2K, S2L, S2M).

2.5. CTPR390-488-treated fibroblasts and fibroblasts from Hsp90aa1 KO mice showed significant reduction of collagen extracellular deposition

The differences among the ultrastructural features of myocardial primary fibroblasts from WT mice, CTPR390–488-treated WT mice and from Hsp90aa1 KO mice were analyzed using electron microscopy technique. Fig 5A and B shows engrossed endoplasmic reticulum because of activated WT fibroblasts synthesizing proteins. WT fibroblasts also exhibited abundant deposition of extracellular collagen fibers (Fig. 5B (1 μm) Fig. 5C (500 μm) pointed with arrows). CTPR390–488-treated fibroblasts showed much thinner endoplasmic reticulum and unstructured collagen fibers extracellularly deposited (Fig. 5D-5F). We did not find CTPR390–488 associated to any cellular organelle (Fig. S3). In the case of myocardial fibroblasts from Hsp90aa1 KO mice, more longitudinal shaped cells (Fig. 5G-5H) with thinner endoplasmic reticulum (Fig. 5I) and the absence of collagen deposition were observed.

2.6. Cell motility is diminished in CTPR390–488-treated fibroblasts and fibroblasts from Hsp90aa1 KO mice

Type I collagen is the major protein component of fibrous connective tissues, and fibroblasts are the cell type primarily responsible for collagen biosynthesis. Cells interacting with collagen network form an arrangement through local matrix. This patterning allows the establishment of tracks for fibroblasts migration and colonization [29–31]. WT myocardial primary fibroblasts were tracked to observe their migration during 20 h after activation with TGFβ (0.3 ng/ml). The average path length per WT cell was 273 ± 24 μm (Fig 6A, G). When cells were treated with 0.2 μM of CTPR390–488 the path length travelled decreased significantly (147 ± 19 μm, ***$p < .001$) (Fig 6C, G); similar to the Hsp90aa1 KO fibroblasts (143 ± 9 μm, ***p < .001) (Fig 6E, G). The collagen secreted to the extracellular media is the main component of the extracellular matrix and the extracellular matrix is the key biological system involved in the progression of disease [32]. The reduction in motility of the CTPR390–488-treated cells can be recovered to initial values culturing the cells on synthetic extracellular matrix (Matrigel) (241 ± 10 μm, ***$p < .001$) (Fig 6D, G). The Hsp90aa1 KO cells on Matrigel also exhibited a certain recovery in their motility but they did not reach the path length values of WT cells (182 ± 24 μm, *$p < .05$) (Fig. 6F, G). The motility of WT control cells was unaltered on the synthetic matrix (242 ± 20 μm) (Fig. 6B, G). Fig. S4 shows the individual cell paths of each assay.

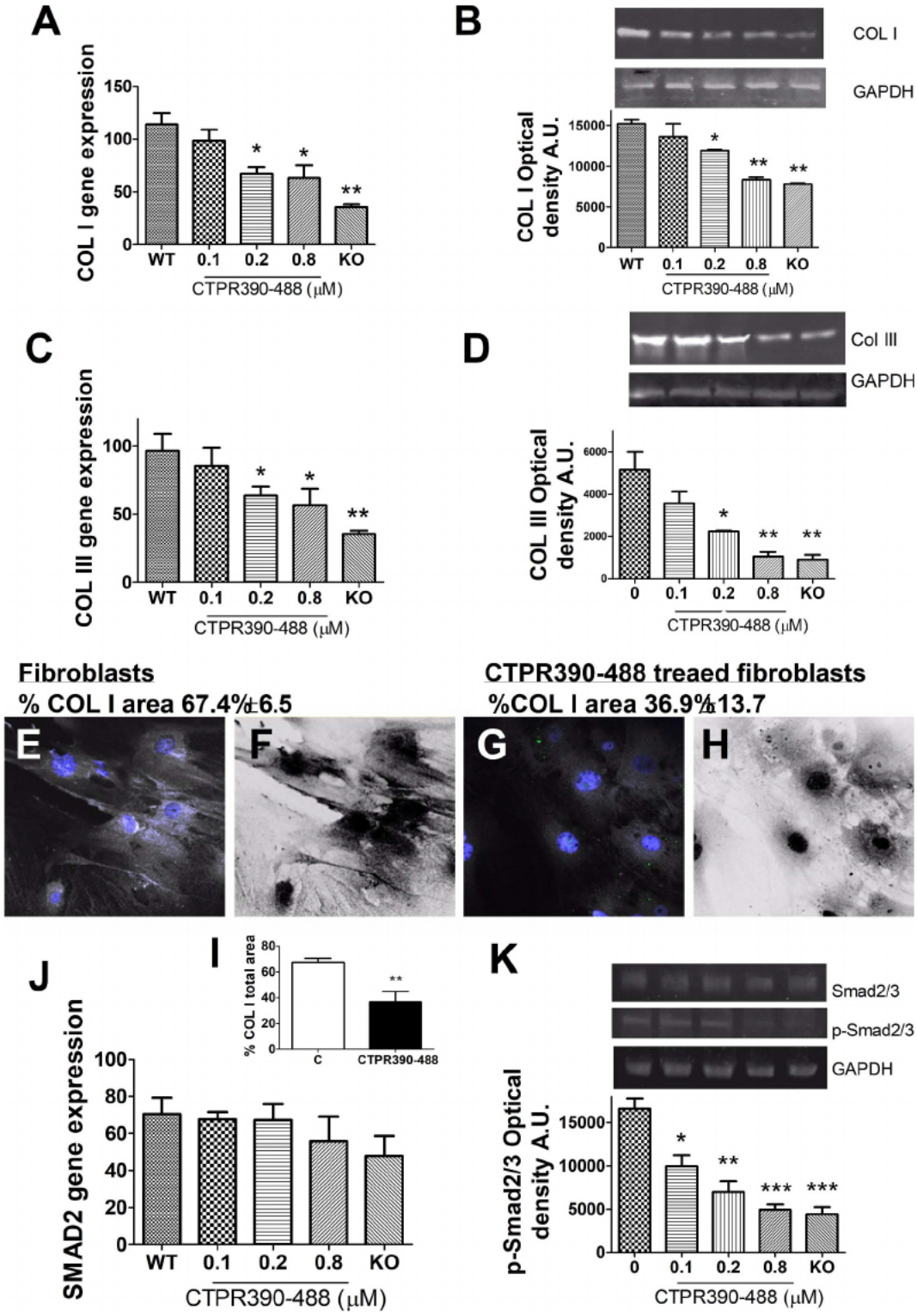

Fig. 4. Gene and protein expression of collagens and Smad2/3 from primary myocardial fibroblast of WT mice (WT), Hsp90aa1 KO mice (KO) and WT with CTPR390–488. A, C, J: Gene expression of collagen I (COL I), collagen III (COL III) and Smad2 presented as relative expression versus 18S ribosomal RNA. B, D, K: Representative Western blots (WB) of COL I, COL III, Smad2/3 and p-Smad2/3 and densitograms of three independent experiments. GAPDH was used as loading control. E, G: Confocal microscopy showing the immunofluorescence detection of collagen I in TGFβ-treated (0.3 ng/ml) primary fibroblasts from WT mice (E), and WT + CTPR390–488-treated fibroblasts (G). Hoechst (blue) was used as a nuclear staining. Anti-rabbit secondary antibody conjugated with Cy5 detected COL I. F, H: Black and white images corresponding to E and G panels respectively. The calculated percentage of collagen I area was the sum of the values in square pixels of the collagen-detected correspondent to graphs F and H (I). The calculated area percentage of the selected pixels was given in calibrated units using ImageJ 1.52e software (Fig. 4I). Data were expressed as mean ± SD of optical density in arbitrary units (A.U.). (*$p < .05$, **$p < .005$, ***p < .001; Mann– Whitney test). (For interpretation of the references to colour in this figure legend, the reader is referred to the web version of this article.)

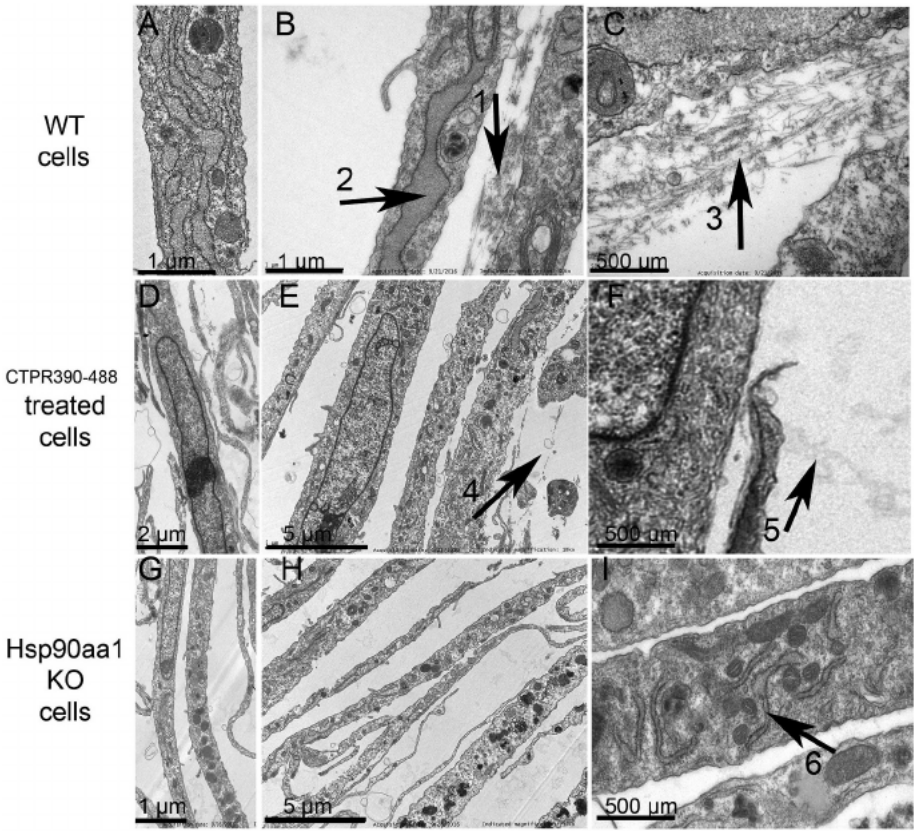

Fig. 5. Representative electron microscopy images of primary myocardial fibroblasts activated with TGFβ (0.3 ng/ml) from control WT mice, WT + CTPR390–488 treated mice and Hsp90aa1 KO mice. A, B: WT cells with engrossed endoplasmic reticulum (ER) (a detail is marked with arrow 2 in panel B). B, C: WT cells with intercellular collagen deposition (arrows 1 panel B and arrow 3 panel C). D, E, F: CTPR390–488 treated WT cells showing normal ER and no structured collagens fibers (arrow 4 panel E, and arrow 5 panel F) and no signs collagen accumulation. G, H, I: cells from Hsp90aa1 KO mice showing thinner morphology, no active ER (arrow 6 panel I) and absence of collagen deposition.

2.7. In vivo administration of CTPR390–488 reduced myocardial fibrosis in Angiotensin II-treated mice

We administrated Ang II to promote the activation of the TGFβ-dependent pro-fibrotic process in the heart of WT and Hsp90 KO mice (see Fig. S5A to check in vivo experimental design). Myocardial Hsp90 chemical inhibition reduces TGFβ signaling cascade [10,33–35]. Mice received a constant infusion of Ang II (0.25 µl per hour, 14 days); and one dose (1 mM) of CTPR390–488 was administrated intraperitoneally. The administration of CTPR390–488 did not alter mice behavior and no sign of discomfort was observed. We measured CTPR390–488 plasma concentrations at different time points for a duration of 2 weeks after its administration, (Fig. S5B-S5C). After 7 days of CTPR390–488 administration collagen I and III reached the lowest levels of gene expression (Fig. S5D-S5E). One week later, the presence of CTPR390–488 was not detected in plasma and the collagen expression increased (Fig. S5D-S5E). Thus, 7 days after CTPR390–488 injection and 14 days after Ang II minipump implantation was a good time-point to determine the effects on gene and protein expression.

TGFβ gene expression in WT + Ang II mice compared to Sham littermates was increased (458.2 ± 39.4 vs 277.3 ± 31.2 $^{**}p < .005$). Furthermore, TGFβ gene expression in WT + Ang II mice treated with CTPR390–488 was also elevated, while Hsp90aa1 KO mice showed lower levels of TGFβ ($^{**}p < .005$) (Fig. 7A). We also evaluated the activation of the canonical signaling mediator of TGFβ, Smad2/3, in heart samples from WT mice treated with Ang II, and we observed significant higher levels of protein phosphorylation compared to control mice (16,470.7 ± 880.3 vs 5380.1 ± 1238.5 a.u. $^{***}p < .001$) and a significant reduction when those mice were treated with CTPR390–488 $^{**}p < .005$) (Fig. 7B). In vivo, collagen I and III expression increased upon Ang II treatment ($p < .05^{*}$) and they both were reduced in WT + Ang II + CTPR390–488 mice ($p < .05^{*}$) compared to Ang II-treated mice (Fig 7C and D). The Hsp90aa1 KO mice did not exhibited changes in TGFβ, COL I, COL III gene expression nor Smad2/3 phosphorylation with Ang II, or Ang II + CTPR390–488 treatment compared to Hsp90aa1 KO sham mice. TGFβ ($^{**}p < .005$), COL I ($^{**}p < .005$), COL III ($^{*}p < .05$) gene expression and Smad2/3 phosphorylation ($^{*}p < .05$) were significantly reduced in Hsp90 KO compared to WT + Ang II mice, (Fig. 7A-7D).

2.8. Systemic CTPR390–488 levels increased in Angiotensin II-treated mice

The endogenous fluorescence of CTPR390–488 allowed its detection in plasma. To obtain the calibration curve of the assay a serial dilution of CTPR390–488 (83.3; 41.7; 20.8; 10.4; 5.2 and 0 µM) was added to plasma of WT mice, and the fluorescence signal obtained for each concentration was adjusted to a second order polynomial (quadratic) curve (Fig. 7E). We checked the CTPR390–488 signal at different time-points (1 h, 5 days, 7 days and 14 days) after CTPR390–488 administration to the different groups of mice in the study (see Fig. S5C); we also generated the calibration curve for each time point (Fig. S5B). Mice subjected to Ang II osmotic infusion for 14 days and CTPR390–488 treatment for 7 days were chosen for the in vivo measurements. The control groups without Ang II showed significant lower levels of CTPR390–488 compared to the Ang II counterparts (0.02 µM ± 0.01 vs 0.80 µM ± 0.10, $^{**}p < .005$; 0.007 µM ± 0.004 vs 0.05 µM ± 0.01, $^{**}p < .005$) (Fig. 7F). In contrast, we observed that the CTPR390–488 plasma levels were higher in the WT + Ang II + CTPR390–488 group compared to KO + Ang II + CTPR390–488 (0.80 µM ± 0.10 vs 0.02 µM ± 0.01, $^{**}p < .005$) (Fig. 7F).

2.9. CTPR390–488 myocardial accumulation

The histological assessment (Fig. 8), showed that CTPR390–488 is accumulated at the left ventricle of WT + Ang II mice treated with CTPR390–488 (Fig. 8D) to a higher extent than their correspondent WT + CTPR390–488 control group (Fig. 8H) or KO + Ang II + CTPR390–488 mice (Fig. 8L) (10.5% ± 1.5, 1.3%% ± 0.4,

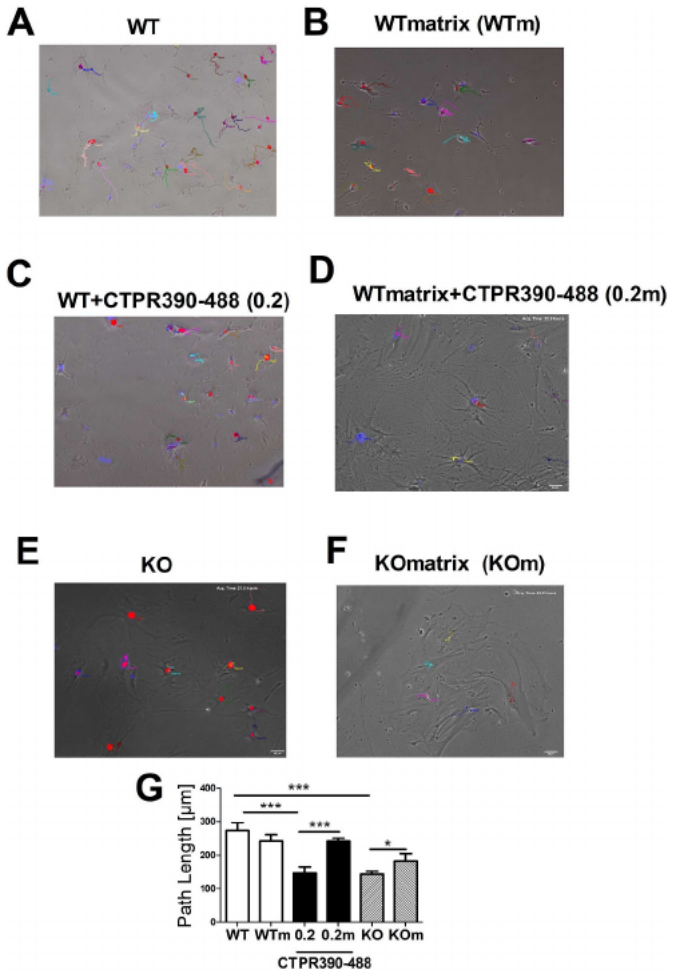

Fig. 6. Path length and cell tracking analysis of myocardial primary fibroblasts followed for 20 h. A, C, E: Representative cell tracks in different colors showing the motility of WT controls (A), WT + CTPR390–488 treated (0.2 μM) cells (C) and Hsp90aa1 KO cells respectively (E). Nuclei marked in red. B, D, F: Path length measurements of cells soaked in matrigel (m) (3 mg/ml) under the same conditions of A, C and E respectively. Nuclei marked in red. G: The path length data obtained from 15 to 32 different areas per assay in triplicate and in three independent experiments. (See S5 Fig for the analysis of the path length travelled (μm) versus time (h:min)). (*p < .05, ***p < .001; Mann– Whitney test). (For interpretation of the references to colour in this figure legend, the reader is referred to the web version of this article.)

0.3% ± 0.2, ***p < .001 see measurements in Fig. S6A-S6D). We checked that both myofibroblasts took up CTPR390–488 in vivo as well as cardiomyocytes (Fig. S6E-S6F). WT + Ang II mice treated with CTPR390–488 presented reduced fibrosis compared to the non-treated mice (Fig. 8B compared to 8C). Fig. 8A showed the combinatory image of myocardial tissue section showing collagen fibers (blue) and the CTPR390–488 detection (green). In the WT + CTPR390–488 mice (Fig. 8E-8H) or the Hsp90aa1 KO + Ang II mice (Fig. 8I-8L) the fibrotic areas were barely detectable in both groups presenting similar appearance.

3. Discussion

The data presented here suggest that the blockade of Hsp90 with an engineered Hsp90 protein inhibitor (CTPR390–488) in myocardial fibroblasts effectively attenuated the canonical TGFβ signaling cascade. The consequences of this modulation promoted lower levels of collagen production and collagen deposition in vitro and in vivo.

We confirmed that the phosphorylation of Smad2/3 signaling effector and the phosphorylation of the non-Smad TGFβ downstream signaling molecules (Akt and Erk) [36] was decreased in the presence of CTPR390–488, while their protein expression is not affected. The preserved folding activity and the unaltered protein expression of Hsp90 client proteins (Akt, Erk, Hsp70 and luciferase) indicated that Hsp90 inhibition by CTPR390–488 was affecting downstream effectors of TGFβRI without altering Hsp90 client proteins. TPR binding domain of the Hsp90 co-chaperones is crucial for the Hsp90 protein-protein interactions and functional complexes formation. CTPR390–488 is an engineered protein presenting an active Hsp90 TPR binding domain that can disrupt the TGFβRI–Hsp90 complex by mimicking the co-chaperone Hsp90-binding domain. Considering the interaction interface observed in the Hsp90-TGFβRI model the conformational change to the open state will disrupt the Hsp90 surface interaction in which the two monomers participate, thus destabilizing Hsp90-TGFβRI complex [7,10]. We hypothesized that CTPR390–488 binding promotes conformational change to open the close Hsp90 dimeric conformation and expulse TGFβRI (Fig. 3J). The crystal structure of the CTPR390–488 domain in complex with the Hsp90 peptide confirmed the mechanism of recognition, mimicking the natural TPR domains that bind the C-terminal sequence of Hsp90 [25]. The specificity of the interaction has been tested by biophysical characterization [15] and in cell culture [16]. The interaction of the extracellular domain of TGFβRI with Hsp90 homodimers occurs when Hsp90 is in a closed conformation [10]. The binding of TPR domain to the C-terminal end of Hsp90 has been shown to promote a conformational change of Hsp90 from the closed state to the open state [26]. Therefore, it is expected that the binding of CTPR390–488 protein to Hsp90 shift its conformational equilibrium toward the open state.

In our previous work [10], we demonstrated that both, Hsp90aa1 and Hsp90ab1 isoforms can be secreted into the extracellular medium and could be part of the Hsp90 dimer bound to TGFβRI. Moreover, CTPR390–488 does not distinguish between Hsp90 isoforms as shown by the reduction in collagens I and III in Hsp90aa1 KO and WT cells. We assume that it also acts on the inducible isoform Hsp90aa1 whose deletion also promotes lowering of TGFβ pro-fibrotic related signaling through phopsho-Smad2/3, as well as collagen I and collagen III production. In any of these cases, Hsp90 lost its chaperon activity. The specific binding of CTPR390–488 to the C-terminal end of Hsp90 displayed binding affinity similar to the endogenous TPR domains and allowed the maintenance of the ATPase dependent Hsp90 chaperone activity.

Cardiac fibroblasts together with cardiomyocytes are the most prevalent cell types in the myocardium [37,38]. Under pathological conditions, cardiac fibroblasts proliferate and increase their motility. The remodeling process includes the colonization of new areas with increase of the total interstitial fibrosis, which in the long term enhances intrinsic myocardial stiffness and results in diastolic dysfunction [39]. The interstitial fibrosis is facilitated by the increased extracellular matrix deposition [36] reduced in Hsp90aa1 KO primary fibroblasts or in the cells treated with the CTPR390–488 protein. Both CTPR390–488 treated-primary fibroblasts and fibroblasts from Hsp90aa1 KO mice exhibited lowered cell motility compared to WT cells. The motility was recovered when cells were cultured on a collagen matrix surface. Thus, the CTPR390–488 protein, likely through its disruption of the Hsp90/TGFβRI complex, promotes a reduction of collagen accumulation in the extracellular matrix, which influences cell motility.

Persistent fibroblast activation is considered responsible for excessive extracellular matrix production and involves tight regulation of the main pro-fibrotic TGFβ signaling cascade. The deletion of Hsp90 affects cell response in myocardial remodeling [9]. Ultrastructural studies of CTPR390–488 treated-fibroblasts interestingly showed intercellular unstructured collagen fibers. We also observed thinner endoplasmic reticulum in the CTPR390–488 treated fibroblasts (as it is the case also for the Hsp90aa1 KO fibroblasts), while the WT fibroblasts presented engrossed endoplasmic reticulum as it would be expected in

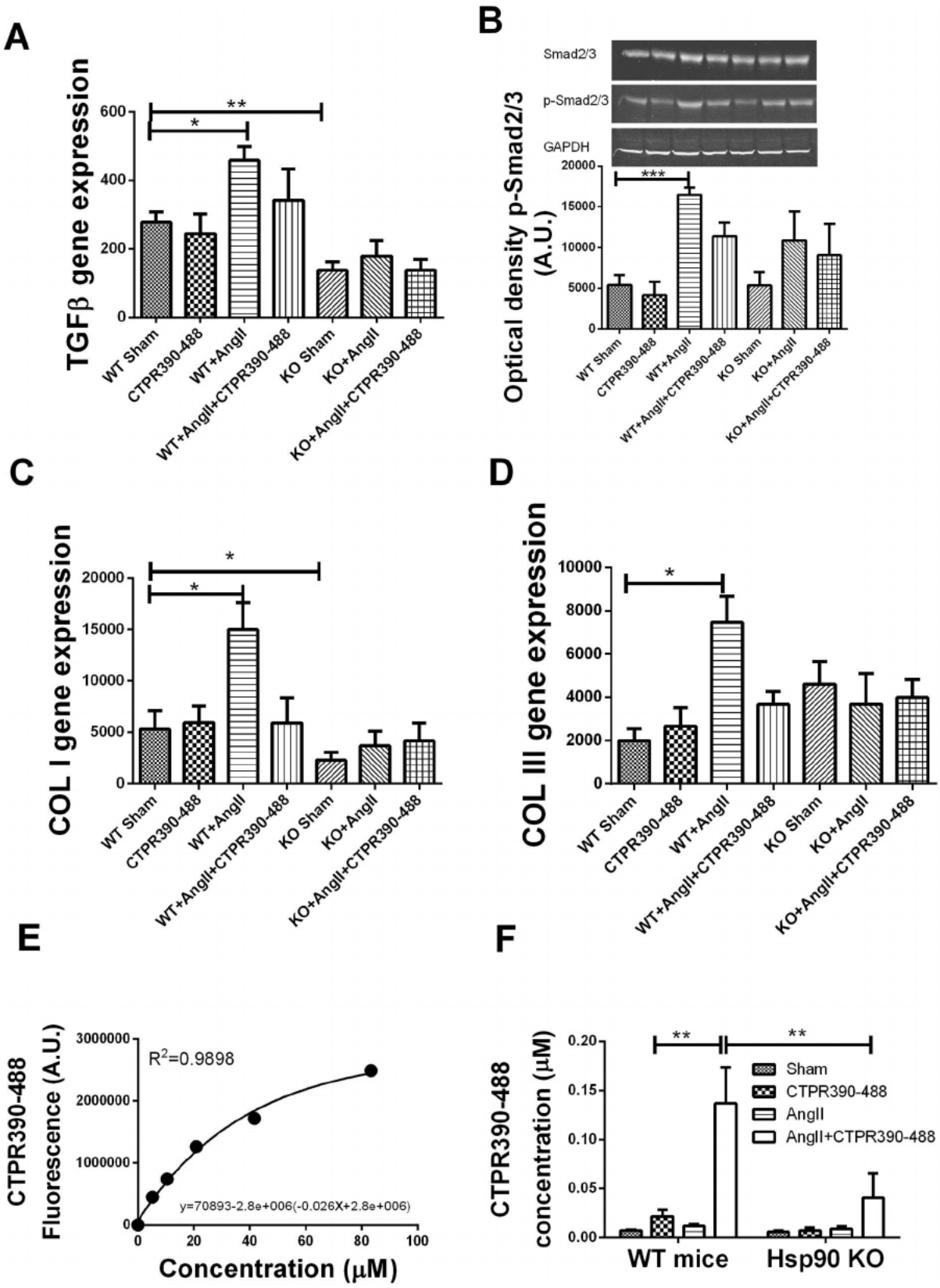

Fig. 7. Gene and protein expressions related to the pro-fibrotic process in the myocardium of WT and KO mice, treated with or without Ang II and CTPR390–488. The samples from left ventricle were extracted from the mice under study: WT, WT + CTPR390–488, WT + Ang II, WT + AngII + CTPR390–488, KO, KO + CTPR390–488, KO + Ang II, KO + AngII + CTPR390–488. (n = 4 per group). A, B, C, D: These panels showed TGFβ gene expression (A), Smad2/3, p-Smad2/3 protein expression and p-Smad2/3 quantification (in arbitrary units A.U.) (B), COL I gene expression (C), and COL III gene expression (D). E: Graph showing the fluorescent signal of CTPR390–488 titration in plasma. F: Graph showing the plasma concentration of CTPR390–488 in the groups of mice under study, n = 4 per group. (*$p < .05$, ***$p < .001$; Mann– Whitney test).

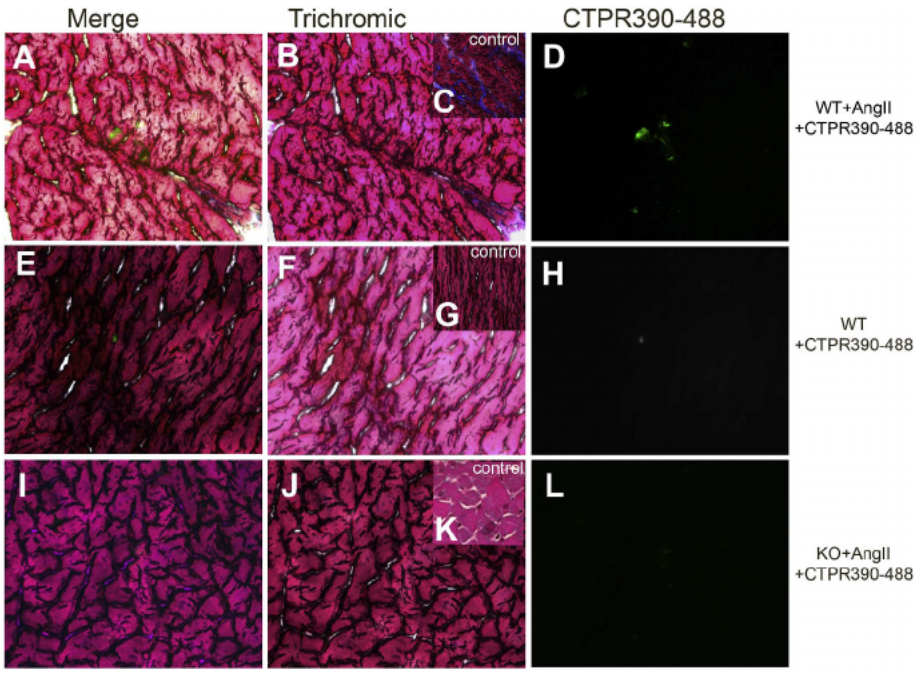

Fig. 8. Representative histological fibrosis of left ventricles transversal sections of Ang II + CTPR390–488 WT mice, CTPR390–488 treated WT mice, and Ang II + CTPR390–488 Hsp90aa1 KO mice. A, E, I: merge of Masson's trichrome staining and confocal images showing accumulation of collagen in blue and detection of CTPR390–488 in green. B, C, F, G, J, K: Collagen staining in blue by Masson's trichrome. D, H, L: Confocal microscopy showing CTPR390–488 in green. C, G and K are the correspondent controls of B, F, and J in the absence of CTPR390–488. (For interpretation of the references to colour in this figure legend, the reader is referred to the web version of this article.)

TGFβ-activated fibroblasts synthesizing collagens.

The rapid advances in understanding the pathophysiology of fibrosis have generated intense interest in developing effective anti-fibrotic therapies for patients with chronic myocardial diseases. With no agents yet approved for this indication, considerable efforts are being invested in developing therapies and novel markers for myocardial fibrosis. These studies using an engineered protein inhibitor, CTPR390–488, is proof of concept to focus our scientific efforts by exploiting the Hsp90 biology. The ability of fluorescently tracking the protein is of special interest in the field of the biomedical use but most importantly is the lack of toxicity when it is internalized by human ductal breast cancer cells [16] or myocardial fibroblasts as we showed herein.

We investigated the in vivo reduction of myocardial fibrosis with the use of the CTPR390–488 protein in WT and Hsp90aa1 KO mice subject to angiotensin II (Ang II) infusion. The systemic administration of Ang II induces cardiac fibroblasts activation including the production and release of the pro-fibrotic cytokine TGFβ [40,41]. TGFβ expression is induced by angiotensin II in kidney, vascular smooth muscle cells, and in cardiac fibroblasts [35]. We utilized the Ang II fibrotic mouse model since angiotensin II receptor blockade were mainly attributed to a reduction in extracellular protein accumulation, most likely mediated through inhibition of TGFβ and its downstream signals [42]. Blockade of the Ang II-TGFβ signaling pathway has consistently been demonstrated to be effective for the prevention of cardiac fibrosis in experimental animals [43–45]. In this study, we show reduction in the accumulation of collagen in the heart of the Ang II treated-mice upon the CTPR390–488 peptide administration or by Hsp90aa1 deletion. This observation suggests that a role of Hsp90 in this fibrotic process and that the inhibition of its TPR binding domain (linked to TGFβRI) is enough to diminish collagen deposition, collagen expression and TGFβ signaling cascade activation.

Moreover, the higher presence of CTPR390–488 protein in the left ventricle and plasma of fibrotic mice compared to control mice indicated its accumulation in fibrotic areas. These observations open the possibility of studying the CTP390–488 protein as a new anti-fibrotic therapy that could also be utilized as a biomarker of the disease. The inhibition of Hsp90 with small molecules produces important side effects in the clinic due to the ATPase activity annulment [46]. We presented here a trackable and potentially safe biomolecule, CPTR390–488, as the first in vivo myocardial anti-fibrotic bio-therapy.

4. Conclusions

Hsp90 inhibition is reached using an engineered protein CTPR390–488, this inhibition likely affects the Hsp90-TGFβRI interaction and it promoted the reduction of key myocardial pro-fibrotic events both in vitro and in vivo. We give an insight into the mechanism of action that would support the hypothesis of Hsp90 and TGFβRI partnership regarding the myocardial fibrotic process. Hsp90 inhibition implies TGFβ signaling deregulation and collagen synthesis reduction. Preservation of Hsp90 folding activity by inhibiting the chaperon with CTPR390–488 offers a new way of targeting left ventricle remodeling without damaging cell homeostasis.

5. Materials and methods

5.1. Protein expression and purification

CTPR390-Cys protein was produced by the introduction of a single C-terminal cysteine in CTPR390 [15] by quick change mutagenesis. CTPR390-cys was expressed as previously described [15,47]. Briefly, CTPR390-Cys gene cloned in pProEx-HTA vector, coding for N-terminal (His)6 tag and ampicillin resistance, was transformed into *Escherichia coli* C41 (DE3). Overnight bacteria culture in 50 ml of Luria–Bertani (LB) media containing 100 μg ml^{-1} of ampicillin was grown to saturation. 10 ml of the saturated culture were diluted into 1 l of LB media supplemented with 100 μg ml^{-1} ampicillin. The cells were grown in an incubator-shaker (250 rpm) at 37 °C to an optical density (OD_{600}) of 0.6–0.8. Expression of CTPR390 was induced with 0.6 mM isopropyl β-d-thiogalactoside (IPTG) followed by 5 h expression at 37 °C. The cells were harvested by centrifugation at 5000 rpm for 20 min. The cell pellets were resuspended in lysis buffer consisting of 300 mM sodium chloride, 50 mM Tris pH 8.0. After 2 min sonication at 30% power using a microtip and Mison sonicator, lysed cells were centrifuged at 16000 rpm for 30 min and the protein supernatant was purified using standard Ni-NTA affinity purification protocol. The N-terminal hexahistidine tag was then cleaved using TEV protease. As a final step, the CTPR390-Cys was dialyzed against 150 mM NaCl, 50 mM phosphate buffer pH 7.4. Protein concentration was measured by UV absorbance at 280 nm, using extinction coefficients at 280 nm calculated from amino acid composition.

5.2. Ligand binding experiments

CTPR390-Cys protein binding affinity to Hsp90 C-terminal peptide was determined by fluorescence anisotropy titrating with increasing amounts of protein into a 50 nM fluorescein-labeled Hsp90 peptide solution [47–49]. Fluorescence anisotropy was recorded exciting at 492 nm with a 5 nm slit width and recording the emission at 516 nm with slit widths of 5 nm. G-factor corrections to account the difference in transmission efficiencies of the two emission channels were applied to calculate anisotropy using PBS buffer as blank solution and a 50 nM fluorescein as a standard solution. Anisotropy values are automatically calculated. The fraction of peptide bound at each point in the binding curve was calculated by the Eq. [15]:

$$\%Bound = \frac{r - r_f}{r_b - r_f}$$

where r is the observed anisotropy of the peptide at any protein concentration, r_f is the anisotropy of the free peptide and r_b is the anisotropy of the peptide bound to the protein in the plateau region of the binding curve. The percentage of peptide bound is plotted versus the protein concentration. The data were fit to a 1:1 binding model using Origin to calculate the dissociation constant.

5.3. CTPR390 labeling with Alexa 488 to obtain CTPR390–488

CTPR390-Cys protein was labeled with the cysteine-reactive maleimide form of Alexa Fluor 488 (Molecular Probes, Inc.) dye through the cysteine at the C-terminal following previously described protocols [24]. Briefly, CTPR390-Cys protein at 100 μM concentration was reduced by incubation with 10 mM 1,4-dithio-DL-treitol (DTT) for 15 min. DTT was removed by gel filtration over a PD-10 column against 150 mM NaCl and 50 mM phosphate (pH 7.0). A solution of Alexa Fluor 488 maleimide in water was added dropwise into the freshly reduced protein in the presence of 1 mM tris(2-carboxyethyl)phosphine to a final 1:5 protein:dye molar ratio. The reactions were allowed to proceed for 4 h at room temperature under a non-reducing atmosphere of N_2 in the dark. The free dye was removed from the reaction mixtures by two consecutive buffer exchange steps over PD-10 columns, followed by concentration and extensive washing using Amicon ultrafiltration tubes with a MWCO of 10-kDa. The extent of labeling was calculated from the absorption spectra of the conjugate and using the extinction coefficient for Alexa Fluor 488 $\varepsilon_{493} = 72{,}000\ M^{-1}\ cm^{-1}$ and the protein extinction coefficient at 280 nm calculated from the amino acid composition.

5.4. Cultured primary cardiac fibroblasts

Adult cardiac fibroblasts from mice C57BL6 strain (wild type) and the transgenic Hsp90aa1 KO were originally isolated directly from enzymatically digested hearts (collagenase, trypsin and DNase) followed by centrifugation and filtration. They were maintained in Dulbecco's Modified Eagle's Medium (DMEM) containing 10% FBS, 10% DBS and 100 U/ml penicillin-streptomycin. The cells (2×10^5) were plated in 35 mm tissue culture dishes and, 4 h later, recombinant TGFβ1 (0.3 ng/ml) (R&D Systems) was added with or without CTPR390–488 (0.2 μM) 24 h later cells were lysed and stored at −80 °C. Results included triplicate of three independent assays. Vimentin marked for positive fibroblasts. For experimental procedures, low passage cells (p2) were seeded onto 35 mm cell culture dishes and incubated at 37 °C in 5% CO_2 for 15–20 h.

5.5. Fluorescence and immunofluorescence assays

The immunofluorescence assays of Hsp90 were performed using TGFβ-treated (0.3 ng/ml for 24 h) primary myocardial fibroblasts and adding 0.2–0.8 μM of CTPR390–488. Paraformaldehyde fixed cells were incubated with mouse primary antibody against Hsp90 (Abcam). We utilized anti-mouse secondary antibody conjugated with Cy3 to detect Hsp90, (Jackson ImmunoResearch, USA). CTPR390–488 was detected with FITC filters and PureBlu Hoechst 33342 (Bio-Rad) was used as nuclear staining dye. LSM-510 laser scanning microscope (Carl Zeiss Inc., Germany) was utilized for these experiments using an objective Plan Apo VC 60 × Oil DIC N2.

5.6. Cell viability assay

Cell viability was assessed in TGFβ-treated cells (0.3 ng/ml for 24 h) in the presence or absence of CTPR390–488. Cells samples were diluted in DMEM medium, PBS 1×, pH 7.4 and 0.4% trypan blue solution (Gibco®-Life technologies) and viability measured by the utilizing Countess®Automated Cell Counter and following the manufacturer's protocol (Countess®Automated, Invitrogen).

5.7. Absorption and fluorescence spectroscopy

The absorbance of the CTPR390–488 treated cells was measured at 488 nm with a NanoDrop instrument (Thermo Scientific) including a calibration curve (3.0, 1.5, 0.8, 0.4, 0.2, 0.1 and 0 μM of CTPR390–488).

Fluorescence measurements of CTPR390–488 signal were performed with 96 well black/clear plates in a Berthold Mithras LB 940 spectrofluorometer. The excitation/emission wavelengths were 485/535 nm. Fluorescence was measured from primary cell lysates and plasma samples containing CTPR390–488.

5.8. Functional refolding assay

To determine Hsp90 chaperone activity we measured the ability of Hsp90 to refold denatured luciferase, which will ultimately catalyze the luciferin reaction. The luciferase renaturation assay was performed in 96-well clear bottom plates containing 25 μg of protein lysate from TGFβ-treated (0.3 ng/ml for 24 h) cells isolated from the left ventricle mice. The refolding reaction was initiated by the addition of the denatured luciferase (1.5 μg/ml, denatured at 46 °C for 10 min, in presence of TGFβ (0.3 ng/ml) to the lysate containing Hsp90 or Hsp90 + CTPR390–488. Once luciferase is renatured after 2 h incubation at room temperature, it will catalyze the luminescent reaction with luciferin. The luciferase activity was measured by addition of Luciferase Assay Reagent (E1501, Promega). The source of Hsp90 was WT primary myocardial fibroblasts and primary myocardial fibroblasts of Hsp90aa1 KO mice. The negative control utilized corresponded to the substrate (heat-denatured luciferase) in the absence of Hsp90 and the positive control corresponded to rabbit reticulocyte lysate (RRL) with high content of Hsp90. Light emission from each micro well was recorded with a 1 s integration time using a Berthold Centro LB 960 plate reader 3 min after addition of the luminescent reagent. Results included triplicate of three independent assays. Buffers and reagents were previously described more in detail by Eachkoti et al. [50].

5.9. Determination of mRNA expressions by Q-PCR

Total mRNA from cells and tissue samples were assayed by Q-PCR; Cell samples were cultured with recombinant TGFβ1 (0.3 ng/ml) with CTPR390–488 and TGFβ for 24 h were obtained by TRIzol extraction (Invitrogen). The mRNA was reverse transcribed using random primers. The quantitative PCR (Q-PCR) were performed with specific TaqMan primers: Hsp90aa1, Hsp90ab1, COL I, COL III, TGFβ1, Smad2 and αSMA. The housekeeping gene was 18S in all cases. The values represented the average of three independent experiments.

5.10. Protein detection by Western Blot

Protein expression was detected by Western blot analysis and

densitogram quantification. Tissue samples were disrupted and lysated. Cell samples were treated with recombinant TGFβ1 (0.3 ng/ml) (Abcam) for 24 h collected, the lysate was resolved on 10% sodium dodecyl sulfate-polyacrylamide (SDS-PAGE) gel and transferred onto polyvinylidene difluoride (PVDF) membranes (Bio-Rad Lab., California, USA). The primary antibodies used were: polyclonal anti Smad2/3 and p-Smad2/3 (Santa Cruz); polyclonal anti GAPDH (Santa Cruz); and polyclonal anti COL I and COL III (Santa Cruz), monoclonal Hsp90 (Abcam). Secondary antibodies conjugated with IRDye 800CW and IRDye 680RD were used for immunodetection. CTPR390–488 protein detection was performed using anti-CTPR390 rabbit antibody purified from the serum from a rabbit immunized with CTPR390 (Unidad de Ensayos Biotecnológicos y Biomédicos, Servicios Científico Técnicos, Universidad de Oviedo).

5.11. Transmission electronic microscopy

Wild type, CTPR390–488 treated, and Hsp90aa1 KO primary cardiac fibroblasts were examined for conventional ultrastructural analysis. Cells were rinsed in 0.1 M phosphate buffer, fixed in 2% osmium tetroxide, dehydrated in acetone, and embedded in araldite (Durcupan, Fluka, Switzerland). For immunogold electron microscopy, myocardial primary fibroblasts were fixed with 4% paraformaldehyde in 0.1 M cacodylate buffer for 30 min at room temperature. Cells were scraped from the dishes, transferred to an Eppendorf tube, and centrifuged for 1 min in a microfuge to obtain cell pellets. The pellets were washed with 0.1 M cacodylate buffer, dehydrated in increasing concentrations of methanol at −20 °C, embedded in Lowicryl K4M at −20 °C, and polymerized with ultraviolet irradiation. Ultrathin sections were mounted on nickel grids and sequentially incubated with 0.1 M glycine in PBS for 15 min, 5% BSA in PBS for 1 h, and the rabbit polyclonal anti-CTPR390–488 antibody diluted 1:50 in PBS containing 1% BSA and 0.1 M glycine for 1 h. After washing, the sections were incubated with goat anti-rabbit IgG coupled to 15 nm gold particles (diluted 1:50 in PBS containing 1% BSA; BioCell, UK). After immunogold labeling. All grids were stained with lead citrate and uranyl acetate and examined with an 80KV electron microscope with Camara Orius SC 100 CCD and Software Gatan. For control, ultrathin sections were treated as described above, but without the primary antibody.

5.12. Cell tracking

Cell track assays were conducted with or without matrigel (3 mg/ml) and activated with TGFβ (0.3 ng/ml). Images were captured overnight every 10 min following cell nuclei (marked with NucBlue Live ReadyProbes Reagent). The distance travelled by cells was obtained by quantification of segmented nuclei. The measurements of the distance travelled by the fibroblasts for 20 h were done on cells plated on tissue culture plates with or without matrigel (3 mg/ml) (Sigma-Aldrich) and activated with TGFβ1 (0.3 ng/ml). The data were obtained from 15 to 32 different areas per assay in triplicate and in three independent experiments. Cell track was captured with an epifluorescence microscope Nikon Ti, objective 10× plan fluor 0.30 NA. Phase contrast / DAPI (387/25 exc-440/25 emis)/ FITC (485/20 exc-521/25 emis). The camera installed was Hamamatsu ORCA R2 and the Software Nis elements with the cell-tracking module was utilized. 0.2 μg/ml of CTPR390–488 was utilized in three independent experiments.

5.13. Simulations of protein-protein interactions

In silico prediction of the interaction between the Hsp90 dimer in close conformation (PDB ID: 2CG9) and the extracellular domain of TGFβRI PDB: 3KFD was described previously [10]. The CTPR390 structure was previously solved in complex with the C-terminal peptide of Hsp90 (PDB ID: 3KD7) [25]. In order to model the ternary complexes including Hsp90-TGFβRI-CTPR390 proteins the flexible C-terminal region of Hsp90 proteins that is recognized by the TPR domain and does not appear in the crystal structured was modeled using UCSF Chimera interface with MODELLER [49].

5.14. Animal studies

Adult (16–20 weeks old) C57BL6 wild type (WT) mice or Hsp90aa1 KO mice were housed in a 22 °C room with 12:12 h light/dark cycle and provided with food and water ad libitum. Mice were divided into 7 groups of $n = 4$ mice per group: WT, WT + CTPR390–488, WT + Ang II, WT + Ang II + CTPR390–488, Hsp90aa1 KO, Hsp90aa1 KO + Ang II and Hsp90aa1 KO + Ang II + CTPR390–488. Live animals' studies were approved by the University of Cantabria Institutional Laboratory Animal Care and Use Committee in compliance with the Guide for the Care and Use of Laboratory Animals (ILAR, 1985) and were conducted in accordance with the "European Directive for the Protection of Vertebrate Animals Used for Experimental and Other Scientific Purposes" (European Communities Council Directive 86/606/EEC).

5.15. Mice handling

In vivo experimental design is shown in Fig. S5A. The experimental time points indicated Ang II time of implantation, CTPR390–488 time of injection and samples collection time-points. Mice were placed on preheated pad set to prevent hypothermia and were anesthetized by inhaled isoflurane in oxygen/nitrous oxide mixtures at 2.0%. Under this anesthesia conditions we performed the following actions:

5.15.1. Subcutaneous implantation of osmotic minipumps

A mid-scapular incision is made, and a subcutaneous pocket is created for the micro-osmotic pump (0.25 μl per hour, 14 days, alzet) to be inserted. The pump was previously filled with an aqueous solution of angiotensin II (0.70 mg). The wound was closed with a suture. Mice were monitored daily for any discomfort and they were euthanized 2 weeks after surgery.

5.15.2. CTPR390–488 intraperitoneal administration

CTPR390–488 (200 μl of 1 mM) intraperitoneal (IP) administration. For the CTPR390–488 intraperitoneal administration mice were anesthetized by 1.0–2.0% inhaled isoflurane in oxygen/nitrous oxide mixtures for 1 min and injected 200 μl of 1 mM of CTPR390–488. Mice did not present any sign of discomfort.

5.15.3. Plasma extraction

Retro-orbital blood collection in mice was performed with animals fully anesthetized. Within 5 min of blood collection plasma was separated by centrifugation at 1000 × *g* and store at −20 °C for posterior use.

5.16. Histological assessment of myocardial fibrosis and CTPR390–488 detection

The hearts from the mice under study described in the section "animal studies" were isolated and fresh frozen after incubation in sucrose 30% for 24 h. The degree of fibrosis was detected in 6 μm sections stained with Masson's trichrome assay. After trichromic staining, bright field images were acquired on an upright fluorescence microscope (Eclipse 80i, Nikon) using a 20 × 0.5 NA or 40 × 0.57 NA objective, a DS-Ri1 colour camera (1280 × 1024 pixels; 0.46 μm & 0.23 μm pixel size). Next, wide field-fluorescence images of the same fields were acquired using excitation (472/30 nm) and emission (520/35) filters. Finally, to reconstitute a RGB colour image we added the green channel from the corresponding fluorescence image to the green channel of the trichrome staining image. The merged images of fluorescence and trichromic staining were obtained with ImageJ after splitting the trichromic RBG colour images in 8bits individual channels (R: red, G: green, B: blue).

5.17. Statistics and graphics program

The data sets were assessed for normality using the Kolmogorov–Smirnov test. Continuous variables were compared using two-tailed Student's *t*-test or Mann–Whitney *U* test. GraphPad Prism 5.03 was utilized as the statistical package and graphics program.

Supplementary data to this article can be found online at https://doi.org/10.1016/j.yjmcc.2018.08.016.

Acknowledgments

We thank Dr. Miguel Lafarga and Dr. Victor Campa for their valuable help.

Funding sources

This work was supported by the Spanish Ministerio de Economia, Industria y Competitividad [BIO2015-72124-EXP] and [BIO2016-77367-R], and the European Research CouncilERC-2014-CoG-648071-ProNANO. The Instituto de Formación e Investigación Marqués de Valdecilla IDIVAL [InnVal 15/31] and [InnVal 17/22], and the FEDER European Union, SODERCAN “Proyecto Puente 2017”.

Disclosures

None declared.

References

[1] X.H. Feng, R. Derynck, Specificity and versatility in tgf-beta signaling through Smads, Annu. Rev. Cell Dev. Biol. 21 (2005) 659–693.
[2] J. La, et al., Downregulation of TGF-beta Receptor-2 Expression and Signaling through Inhibition of Na/K-ATPase, PLoS One (2016) 11(12).
[3] M.M. Villarreal, et al., Binding Properties of the Transforming Growth Factor-beta Coreceptor Betaglycan: Proposed Mechanism for Potentiation of Receptor complex Assembly and Signaling, Biochemistry 55 (49) (2016) 6880–6896.
[4] H. Noh, et al., Heat shock protein 90 inhibitor attenuates renal fibrosis through degradation of transforming growth factor-beta type II receptor, Lab. Investig. 92 (11) (2012) 1583–1596.
[5] A.K. Reka, et al., Identifying inhibitors of epithelial-mesenchymal transition by connectivity map-based systems approach, J. Thorac. Oncol. 6 (11) (2011) 1784–1792.
[6] M. Tomcik, et al., Heat shock protein 90 (Hsp90) inhibition targets canonical TGF-beta signalling to prevent fibrosis, Ann. Rheum. Dis. 73 (6) (2014) 1215–1222.
[7] R. Datta, et al., Hsp90/Cdc37 assembly modulates TGFbeta receptor-II to act as a profibrotic regulator of TGFbeta signaling during cardiac hypertrophy, Cell. Signal. 27 (12) (2015) 2410–2424.
[8] S.J. Myung, et al., Heat shock protein 90 inhibitor induces apoptosis and attenuates activation of hepatic stellate cells, J. Pharmacol. Exp. Ther. 330 (1) (2009) 276–282.
[9] R. Datta, et al., Myocyte-Derived Hsp90 Modulates Collagen Upregulation via Biphasic Activation of STAT-3 in Fibroblasts during Cardiac Hypertrophy, Mol. Cell. Biol. 37 (6) (2017) 00611–00616.
[10] R. Garcia, et al., Extracellular heat shock protein 90 binding to TGFbeta receptor I participates in TGFbeta-mediated collagen production in myocardial fibroblasts, Cell. Signal. 28 (10) (2016) 1563–1579.
[11] C. Vancheri, et al., Idiopathic pulmonary fibrosis: a disease with similarities and links to cancer biology, Eur Respir J. 35 (3) (2010) 496–504, https://doi.org/10.1183/09031936.00077309 Mar.
[12] Y.L. Boersma, A. Pluckthun, DARPins and other repeat protein scaffolds: advances in engineering and applications, Curr. Opin. Biotechnol. 22 (6) (2011) 849–857.
[13] A. Pluckthun, Designed ankyrin repeat proteins (DARPins): binding proteins for research, diagnostics, and therapy, Annu. Rev. Pharmacol. Toxicol. 55 (2015) 489–511.
[14] L. Regan, M.R. Hinrichsen, C. Oi, Protein engineering strategies with potential applications for altering clinically relevant cellular pathways at the protein level, Expert Rev. Proteomics 13 (5) (2016) 481–493.
[15] A.L. Cortajarena, et al., Protein design to understand peptide ligand recognition by tetratricopeptide repeat proteins, Protein Eng Des Sel 17 (4) (2004) 399–409.
[16] A.L. Cortajarena, F. Yi, L. Regan, Designed TPR modules as novel anticancer agents, ACS Chem. Biol. 3 (3) (2008) 161–166.
[17] A.L. Cortajarena, S.G. Mochrie, L. Regan, Modulating repeat protein stability: the effect of individual helix stability on the collective behavior of the ensemble, Protein Sci. 20 (6) (2011) 1042–1047.
[18] A.L. Cortajarena, et al., Designed proteins to modulate cellular networks, ACS Chem. Biol. 5 (6) (2010) 545–552.
[19] M.E. Jackrel, et al., Screening libraries to identify proteins with desired binding activities using a split-GFP reassembly assay, ACS Chem. Biol. 5 (6) (2010) 553–562.
[20] D. Bai, et al., Cytoplasmic translocation of HuR contributes to angiotensin II induced cardiac fibrosis, Biochem. Biophys. Res. Commun. 463 (4) (2015) 1273–1277.
[21] Y. Sun, et al., Angiotensin II, transforming growth factor-beta1 and repair in the infarcted heart, J. Mol. Cell. Cardiol. 30 (8) (1998) 1559–1569.
[22] K.T. Weber, Extracellular matrix remodeling in heart failure: a role for de novo angiotensin II generation, Circulation 96 (11) (1997) 4065–4082.
[23] Y. Zhang, et al., Overexpressed connective tissue growth factor in cardiomyocytes attenuates left ventricular remodeling induced by angiotensin II perfusion, Clin. Exp. Hypertens. 39 (2) (2017) 168–174.
[24] A.L. Cortajarena, et al., Non-random-coil behavior as a consequence of extensive PPII structure in the denatured state, J. Mol. Biol. 382 (1) (2008) 203–212.
[25] A.L. Cortajarena, J. Wang, L. Regan, Crystal structure of a designed tetratricopeptide repeat module in complex with its peptide ligand, FEBS J. 277 (4) (2010) 1058–1066.
[26] J. Li, J. Soroka, J. Buchner, The Hsp90 chaperone machinery: conformational dynamics and regulation by co-chaperones, Biochim. Biophys. Acta 3 (2012) 624–635.
[27] K.H. Wrighton, X. Lin, X.H. Feng, Critical regulation of TGFbeta signaling by Hsp90, Proc. Natl. Acad. Sci. U. S. A. 105 (27) (2008) 9244–9249.
[28] H. Dong, et al., Blockade of extracellular heat shock protein 90alpha by 1G6-D7 attenuates pulmonary fibrosis through inhibiting ERK signaling, Am J Physiol Lung Cell Mol Physiol 313 (6) (2017) L1006–L1015.
[29] P. Friedl, et al., Migration of highly aggressive MV3 melanoma cells in 3-dimensional collagen lattices results in local matrix reorganization and shedding of alpha2 and beta1 integrins and CD44, Cancer Res. 57 (10) (1997) 2061–2070.
[30] P.P. Provenzano, et al., Collagen reorganization at the tumor-stromal interface facilitates local invasion, BMC Med. 4 (1) (2006) 38.
[31] R.T. Tranquillo, Self-organization of tissue-equivalents: the nature and role of contact guidance, Biochem. Soc. Symp. 65 (1999) 27–42.
[32] T. Ishimoto, et al., Activation of Transforming Growth factor Beta 1 Signaling in Gastric Cancer-associated Fibroblasts increases their Motility, via Expression of Rhomboid 5 Homolog 2, and Ability to Induce Invasiveness of Gastric Cancer Cells, Gastroenterology 5 (17) (2017) (35398–2).
[33] J.A. de la Mare, T. Jurgens, A.L. Edkins, Extracellular Hsp90 and TGFbeta regulate adhesion, migration and anchorage independent growth in a paired colon cancer cell line model, BMC Cancer 17 (1) (2017) 017–3190.
[34] Z. Sibinska, et al., Amplified canonical transforming growth factor-beta signalling via heat shock protein 90 in pulmonary fibrosis, Eur. Respir. J. 49 (2) (2017) 01941–02015.
[35] S.B. Lee, et al., Modulation of heat shock protein 90 affects TGF-beta-induced collagen synthesis in human dermal fibroblast cells, Tissue Cell 48 (6) (2016) 616–623.
[36] C. Bonnans, J. Chou, Z. Werb, Remodelling the extracellular matrix in development and disease, Nat Rev Mol Cell Biol 15 (12) (2014) 786–801.
[37] P. Camelliti, T.K. Borg, P. Kohl, Structural and functional characterisation of cardiac fibroblasts, Cardiovasc. Res. 65 (1) (2005) 40–51.
[38] I. Banerjee, et al., Determination of cell types and numbers during cardiac development in the neonatal and adult rat and mouse, Am. J. Physiol. Heart Circ. Physiol. 293 (3) (2007) 29.
[39] J. Diez, et al., Clinical aspects of hypertensive myocardial fibrosis, Curr. Opin. Cardiol. 16 (6) (2001) 328–335.
[40] I. Manabe, T. Shindo, R. Nagai, Gene expression in fibroblasts and fibrosis: involvement in cardiac hypertrophy, Circ. Res. 91 (12) (2002) 1103–1113.
[41] S. Rosenkranz, TGF-beta1 and angiotensin networking in cardiac remodeling, Cardiovasc. Res. 63 (3) (2004) 423–432.
[42] A.E. El-Agroudy, et al., Effect of donor/recipient body weight mismatch on patient and graft outcome in living-donor kidney transplantation, Am J Nephrol 23 (5) (2003) 294–299.
[43] D.S. Lim, et al., Angiotensin II blockade reverses myocardial fibrosis in a transgenic mouse model of human hypertrophic cardiomyopathy, Circulation 103 (6) (2001) 789–791.
[44] C.M. Yu, et al., Effects of combination of angiotensin-converting enzyme inhibitor and angiotensin receptor antagonist on inflammatory cellular infiltration and myocardial interstitial fibrosis after acute myocardial infarction, J. Am. Coll. Cardiol. 38 (4) (2001) 1207–1215.
[45] P. Teekakirikul, et al., Cardiac fibrosis in mice with hypertrophic cardiomyopathy is mediated by non-myocyte proliferation and requires Tgf-beta, J. Clin. Invest. 120 (10) (2010) 3520–3529.
[46] D.S. Hong, et al., Targeting the molecular chaperone heat shock protein 90 (HSP90): lessons learned and future directions, Cancer Treat. Rev. 39 (4) (2013) 375–387.
[47] P. Couleaud, et al., Designed Modular Proteins as Scaffolds to Stabilize Fluorescent Nanoclusters, Biomacromolecules 16 (12) (2015) 3836–3844.
[48] A.L. Cortajarena, L. Regan, Ligand binding by TPR domains, Protein Sci. 15 (5) (2006) 1193–1198.
[49] T.Z. Grove, L. Regan, A.L. Cortajarena, Nanostructured functional films from engineered repeat proteins, J. R. Soc. Interface 10 (83) (2013) 6.
[50] R. Eachkoti, et al., Identification and characterisation of a novel heat shock protein 90 inhibitor ONO4140, Eur. J. Cancer 50 (11) (2014) 1982–1992.